Available online at www.sciencedirect.com
SCIENCE DIRECT®
Journal of Solid State Chemistry 177 (2004) 2565–2574
JOURNAL OF SOLID STATE CHEMISTRY
http://elsevier.com/locate/jssc

Mechanochemical synthesis of nanostructured fluorapatite/fluorhydroxyapatite and carbonated fluorapatite/fluorhydroxyapatite

I. Nikčević,[a] V. Jokanović,[a,*] M. Mitrić,[b] Z. Nedić,[c] D. Makovec,[d] and D. Uskoković[a]

[a] *Advanced Materials and Technologies, Institute of Technical Sciences of the Serbian Academy of Sciences and Arts, Knez Mihailova St. 35/IV, Belgrade 11 000, Serbia and Montenegro*

[b] *Laboratory for Theoretical and Condensed Matter Physics, The Vinča Institute of Nuclear Sciences, P. O. Box 522, Belgrade 11001, Serbia and Montenegro*

[c] *Faculty of Physical Chemistry, University of Belgrade, Studentski trg 12-16, P. O. Box 137, Belgrade, Serbia and Montenegro*

[d] *Jožef Stefan Institute, Jamova 39, Ljubljana SI-1000, Slovenia*

Received 21 October 2003; received in revised form 27 January 2004; accepted 22 March 2004

Abstract

Powder mixture of $Ca(OH)_2$-P_2O_5-CaF_2 were milled in planetary ball mill. A carbonated fluorhydroxyapatite, FHA $Ca_{10}(PO_4)_{1-y}(CO_3)_y(PO_4)_5(OH)_{2-2x1}(F)_{2x1}$ was formed after 5 h of milling and carbonated fluoroapatite $Ca_{10}(PO_4)_{1-y}(CO_3)_y(PO_4)_5(F)_2$ was formed after 9 h of milling. Complete transformation of the carbonated form of FA into then single phase of FA occurred after 9 h milling and thermally treating. The various experimental techniques like X-ray Diffraction (XRD), Differential Thermal Analysis (DTA), Infrared Spectroscopy (IR), Transmission Electron Microscopy and Scanning Electron Microscopy (SEM) were used to characterize the synthesized powders and to postulate reaction mechanisms' steps- transformations of reactants involved.

Keywords: Fluorapatitie; Carbonated fluorhydroxyapatite; Hydroxyapatite; Mechanochemical synthesis

1. Introduction

Calcium apatites, also known as hydroxyapatite (HA), $Ca_{10}(PO_4)_6(OH)_2$ and fluoroapatite (FA), $Ca_{10}(PO_4)_6F_2$, are the main sources of inorganic phosphorus in nature [1]. Their chemical compositions, biocompatibility and bioresorbility is roughly equivalent to inorganic matrix of the bone [2–4], and hence the HA is accepted as a potential bone substitute material in orthopedics and dentistry. The inorganic matrix of the bone is based on HA doped with different quantities of cations as Na^+, K^+ and Mg^{2+}, and anions as CO_3^{2-}, SO_4^{2-} and F^-. Among them, CO_3^{2-} and F^- play one of the leading roles because of their influence on the physical and biological properties of HA [3,5,6]. Namely, fluorine as a micro-element is necessary for the normal dental and bone formation in the body [7].

Solubility of carbonated fluorapatites increases with increasing CO_3^{2-} concentration in chemical and biological media [4]. This is very important since the solubility of fluorohydroxyapatite (FHA) decreases with increasing F^- concentration down to the minimal solubility, characteristic of FA [8,9]. In this way lower solubility of FHA/FA can be compensated. Namely, an increase of F^- concentration in FHA, up to that in FA, results in better chemical and thermal stability of FHA compared to HA [7–10]. So, the designed carbonated fluoro-hydroxyapatite/fluoroapatite system, its phase contents, could be easily optimized to meet the requirements set for the reparation of bones, teeth, etc. [7–10].

Because of these characteristics, HA, FA, carbonated HA/FHA/FA, as well as their combinations have been extensively studied, applying different synthesis methods (precipitation, sol–gel, solid-state, hydrothermal precipitation) [11–23]. Unlike mechanochemical synthesis of HA, reported in Ref. [24–29], the mechanochemical synthesis of FHA, FA, and carbonated FA/FHA have not yet been investigated. Therefore, the aim of this

*Corresponding author. Fax: +381-11-185263.
E-mail address: vukoman@itn.sanu.ac.yu (V. Jokanović).

0022-4596/$ - see front matter © 2004 Elsevier Inc. All rights reserved.
doi:10.1016/j.jssc.2004.03.024

article was to study the mechanochemical synthesis of carbonated FA/FHA and FA/FHA, its mechanism, and the crystallization of phases obtained in the process.

2. Material and methods

Calcium hydroxide, $Ca(OH)_2$, phosphorous oxide, P_2O_5, and calcium fluoride, CaF_2, powders (all p.a., Merck) were used for the synthesis of carbonated FHA/FA and FA. The appropriate amounts of the starting materials were mixed. The mole ratio of calcium hydroxide to phosphorous oxide and calcium fluoride was 9:3:1. The powders were put into agate vials with alumina balls, 1 cm in diameter. Mechanochemical reaction was performed in a planetary ball mill (RETCH) at a rotating speed of ~230 rpm. The mass ratio of balls to reactants was 34, whereby the overall ball mass was 452 g. Milling time varied from 1 to 9 h.

Synthesized products were analyzed by X-ray diffractometry, XRD (Philips PW 1050), using Cu$K\alpha_{1,2}$ Ni-filtered radiation. The patterns were registered in the 2θ range 9°–67° with a scanning step size of 0.02°. For structure refinement, the Reitveld full profile method [30] was applied, using the Koalarie computer software [31] to model diffraction maxima by combining fundamental parametric approach with modern algorithm. Crystalline structure and operating X-ray diffractometer parameters were used for the purpose.

The morphology and the agglomerate size distribution of the milled powders were studied by scanning electron microscopy, SEM (JEOL JSM-5300). Prior to SEM analysis, the as-prepared samples were suspended in ethanol and dispersed ultrasonically for 10 min. Subsequently, the powder samples were coated with gold using PVD. Diameter of over 200 particles/agglomerates was measured and obtained results were statistically treated to estimate the average particle/agglomerate size distribution characteristics. Chemical homogeneity of samples was analyzed using Energy Dispersive Spectrometer, EDS, with a Si (Bi) X-ray detector. Analysis is done by QX 2000 system (Oxford Instruments, UK) connected to scanning electron microscope and computer multi-channel analyzer. The measurements were performed to detect: P, Ca and F. This equipment was used to analyze X-rays from 0.5 to 20 keV with 10 eV per channel. Semi-quantitative analyses show that these elements are present in different ratios in various parts of the sample. The YAF (Link Company) software package was used to compare intensities of reflected X-ray light from the surface of the analyzed sample and the surfaces of the corresponding standards (the package contains standards for elements with atomic numbers equal to or higher than 8). Good results were obtained for elements with atomic numbers greater than 10.

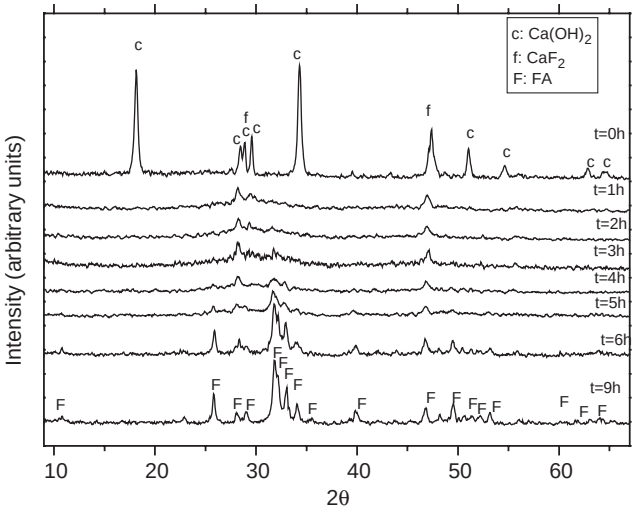

Fig. 1. XRD-patterns of untreated and mechanochemically treated mixture of $Ca(OH)_2$–P_2O_5–CaF_2.

In addition to EDS analysis, F^- ions were also analyzed by Ion Selective Method (Orion fluoride electrode, model 94-09A) with Corning Model 10 Expanded pH meter.

The powder morphology was studied thoroughly by transmission electron microscopy, TEM (JEOL JEM 2000 FX). As for the SEM, the samples were dispersed ultrasonically in acetone. The suspensions were placed on transparent carbon foils, supported by copper grids.

Mechanochemically treated samples were further investigated by differential thermal analysis, DTA (AMINCO). The analysis was done in air, with a heating rate of 10°C/min, and by infrared absorption spectroscopy. IR spectra of powder samples were recorded on a PERKIN ELMER 983G instrument, using KBr pastille technique.

3. Results

3.1. X-ray powder diffraction

Fig. 1 shows the XRD patterns of $Ca(OH)_2$–P_2O_5–CaF_2 powder mixture, mechanically alloyed for 1–9 h. An XRD-pattern of the mixture before milling is given in the same figure for comparison. The X-ray pattern of the sample, milled for 1 h, shows the most intense peaks for CaF_2 [(111) at $2\theta = 28.2°$; (220) at $2\theta = 47.1°$],[1] while the most intense ones for $Ca(OH)_2$ disappeared.[2] The X-ray patterns of the samples milled for 2–4 h confirm a continuation of the mechanochemical process.

[1] JCPDS File No. 35-0816 (CaF_2), International Center for Diffraction Data.

[2] JCPDS File No. 04-0733–$Ca(OH)_2$, International Center for Diffraction Data.

Table 1
Ion positions and refinement parameters

	x	y	z	B (Å^2)
$F^-(\bar{6})$	0	0	1/4	3.7 (0.4)
Ca^{2+} (6h)	0.2385 (4)	0.9888 (5)	1/4	1.31 (7)
Ca^{2+} (4f)	1/3	2/3	0.5005 (8)	0.9 (1)
P^{5+} (6h)	0.3984 (6)	0.3699 (6)	1/4	1.6 (1)
O^{2-}(1) (6h)	0.3229 (11)	0.4802 (10)	1/4	3.1 (3)
O^{2-}(2) (6h)	0.5878 (11)	0.4683 (10)	1/4	2.5 (2)
O^{2-}(3) (12i)	0.3338 (7)	0.2529 (8)	0.43175 (8)	3.1 (2)
	$R_{wp} = 9.5\%$		$R_B = 7.8\%$	

First, weakly defined peaks for FA[3] appeared for the sample milled for 5 h. The clear resolution of all characteristic diffraction peaks for FA can be seen for the sample milled for 6 h. Further increase in milling time up to 9 h resulted in further increase in crystalline order of the FA phase—further sharpening of the principal diffraction peaks (Fig. 1).

3.2. Structure refinement

The XRD data were used for additional refinement of the sample structures by analyzing the space group $P6_3/m$ (No. 176) with the following ion positions (30): F^- is located at the crystallographic position 2*a* [001/4] with the local symmetry $\bar{6}$; P^{5+} is located at the crystallographic position 6*h* [*xy*1/4] with the local symmetry *m*; Ca^{2+} is located at two crystallographic positions—one at 6*h* [*xy*1/4] with the local symmetry *m* and the other is at the position 4*f* [1/3 2/3 *z*] with the local symmetry 4*f*; O^{2-} is located at two different 6*h* positions [*xy*1/4] with the local symmetry *m*, and at the general crystallographic position 12*i* [*xyz*] with the local symmetry 1. Error *R* factors ($R_{wp} = 9.5\%$, $R_B = 7.8\%$), as shown in Table 1, verify quality of refinement as their values are below 10%. Atomic parameters, fixed atomic positions and those obtained by refinement are given in Table 1. The structural parameters were refined with individual thermal factors and occupation factors. Thermal *B* factors (A^2) given in Table 1 show no unusual behavior. They are in agreement with their ionic/atomic diameter for different ionic species (lighter ions have greater *B* factors and heavier ions have smaller *B* factors).

Fig. 2a shows the nearest neighbors of F^- ion in the carbonate fluoroapatite/fluoroapatite structure. It can be seen that there are three $CaII^{2+}$ in the immediate neighborhood of F^- ion at the distance of 2.3 Å. These $CaII^{2+}$ ions form the vertices of an equilateral triangle with the F^- ion at the center. In the outer coordination sphere there are three of each $CaII^{2+}$, P^{5+}, and O^{2-} ions mutually forming the vertices of a triangle. The distance between F^- and P^{5+} is 3.6 Å, and between P^{5+} and O^{2-}(1) is 3.9 Å. There are O^{2-}(3) ions below and above plane containing F^- and $CaII^{2+}$. Oxygen ions occupy vertices of a dodecahedron. The distances between F^- and O^{2-}(3) ions are 3.1 Å, while it is 1.5 Å between P^{5+} and O^{2-}(3). Fig. 2b shows a fragment of the crystal lattice compared with the unit cell.

Analysis of microstructural parameters shows that there is a difference in the crystallite size (21 and 31 nm, respectively) and in the microstrain (0.3(1)% and 0.0(1)%, respectively) for samples milled for 6 and 9 h. According to Panda et al., $CaII^{2+}$ has higher atomic size compared to CaI^{2+} [19]. When OH^- ions were substituted with F^- there is more distortion in the structure because of the larger ionic radii of F^-. At the end of the process, the F^- ion occupies a large space in the center of the lattice, thus forming stable FA structure.

Observed and calculated XRD-patterns of mixture $Ca(OH)_2$–P_2O_5–CaF_2 mechanochemically treated for 9 h are given in Fig. 3.

The unit cell parameters *a* and *c* of FA/FHA for the samples milled for 6 and 9 h, are given in Table 2. According to the results summarized in Table 2, prolonged milling caused a decrease in *a* and an increase in *c* lattice parameters.

The increase in *c* is negligible, which is in agreement with the literature data, while the decrease in *a* indicates that only partial fluorination took place during mechanochemical treatment leading to the formation of FHA (for the milling time of 6 h, $a = 0.9414$ nm).[4] For the sample milled for 9 h, the *a* value agrees with the literature data, indicating formation of carbonated FA (Table 2).

3.3. IR spectroscopy

IR spectra of the samples milled for 1 h compared with the IR spectrum of the starting mixture reveal a substantial change in the system phase composition which occurred during that first hour of milling. All characteristic bands corresponding to the system components, at wave numbers 565, 875, 918, 1090, 1442, and 1626 cm^{-1}, are of different shape. Also, appearance of new bands at 726 and 758 cm^{-1}, and disappearance of the band at 818 cm^{-1} is evident (Fig. 4).

The bands at 565 and 1090 cm^{-1} correspond to the asymmetrical v_4 and v_3 stretching vibrations of the phosphate group, while the band at 1442 cm^{-1} corresponds to the v_3 starching vibrations of the carbonate group [32,33].

The band at 1626 cm^{-1} corresponds to the bending vibration of the hydroxyl (OH^-) group, In the case of

[3] JCPDS File No. 15-876 (FA), International Center for Diffraction Data.

[4] JCPDS File No. 31-0267–carbonate fluorohydroxyapatite International Center for Diffraction Data.

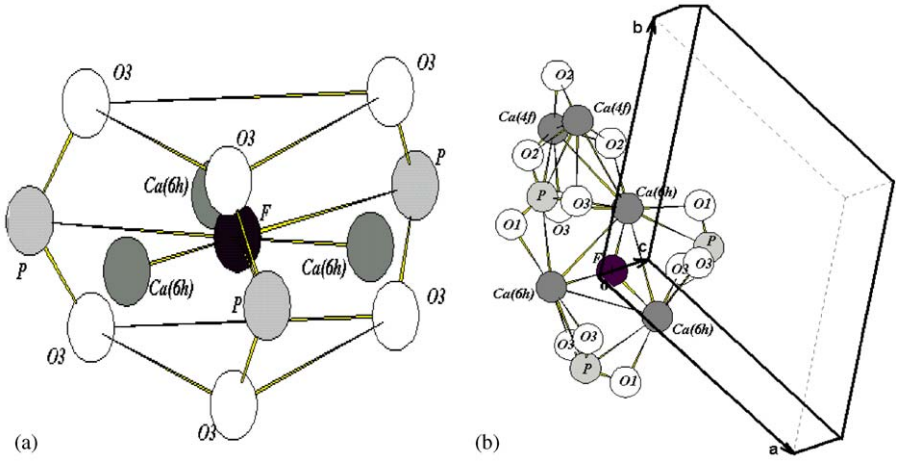

Fig. 2. (a) Nearest neighbors of F^- ion in the carbonate fluoroapatite/fluoroapatite structure; (b) fragment of crystal lattice compared with unit cell.

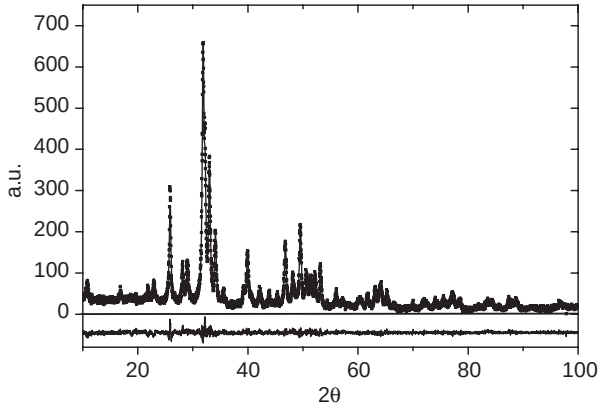

Fig. 3. Observed and calculated XRD-patterns of mixture $Ca(OH)_2$–P_2O_5–CaF_2 mechanochemically treated for 9 h.

Table 2
List of crystallite size and cell parameters of FA calculated from the XRD data

Cell parameters and crystallite size	Sample				
	FA ($t = 4$ h)	FA ($t = 5$ h)	FA ($t = 6$ h)	FA ($t = 9$ h)	JCPDS 15-876
A (nm)	0.9467	0.9441	0.9414(4)	0.9379(2)	0.9368
C (nm)	0.6821	0.6873	0.6879(3)	0.6885(1)	0.6884
cd (nm)	5	10	22	31	

samples milled for 4 h or longer, a new band appears at 603 cm^{-1}, which corresponds to the asymmetric v_4 vibration of the phosphorus group (PO_4^{3-}) [32,33].

For the samples milled for 5 h or longer, a doublet appears at 1420 and 1455 cm^{-1} that corresponds to v_3 vibrations of the carbonate group (CO_3^{2-}). The band at 875 cm^{-1} assigned to the HPO_4^{2-} group vibration [32,33], disappears after 4 h of milling. The band at 918 cm^{-1} ascribed to HPO_4^{2-} disappears for the samples milled for 5 h or longer. In the case of samples milled for 6 and 9 h, the band at 963 cm^{-1} corresponding to the v_4 vibration of the PO_4^{3-} group appears as a result of the HPO_4^{2-} group deprotonation (Fig. 4, Table 3).

Also, for samples milled from 2 to 6 h, the band at 726 cm^{-1} corresponds to the shifting OH^- liberation mode (see Fig. 4). This is caused by the increase of F^- content of in the (OH^-, F^-) chain of apatite with predominant configuration of …FHO:OHF… [34]. According to literature [34], this configuration is typical for samples in which almost 50% of OH^- ions being replaced by F^- ions. In addition to this, the obtained mixture of calcium hydroxyapatite and fluoroapatite is approximately equimolar for all the samples in which only the band at 726 cm^{-1} is observed. Besides the band at 726 cm^{-1}, for the sample milled 6 h and after thermally treated at 1100°C, the band at 758 cm^{-1} appears, while for sample milled 9 h and thermally treated at 1100°C, only the band at 758 cm^{-1} appears. Fig. 5a and Table 3 compares the IR spectra of mechanochemically treated products before and after the thermal treatment. According to literature, appearance of the band at 758 cm^{-1} shows that the configuration …FHOF… is predominant [34].[5] This is also in

[5] According to the literature [34] the (OH^-, F^-) chain of apatite should contain at least three types of [OH^-] and a possible fourth one with distinguishable vibrational energies: (1) the "normal" [OH^-] in an extended [OH^-] chain (configuration …OHOHOH…), (2) "tail to tail" configuration HO:OH, (3) the F^- bonded [OH^-] in the symmetrical configuration …OHFHO…, and finally (4) in F^- rich chains containing only a few [OH^-], in which the F^- bonded [OH^-] has an asymmetrical configuration …FFOHFF….

In general H, F apatite chains have …FHO(OH)nHO:OH(OH)-nOHF… configuration where n depends on OH^- and F^- ratio within the apatite. n decreases with increasing F^- ion content, and there is a …FHOHO:OHOHF… configuration for $n = 0$. With further increase of F^- vs. OH^- ion content in apatite, the chain reduces the number of OH^- ions until the formation of …FHO:OHF… and …FOHF… chain configuration.

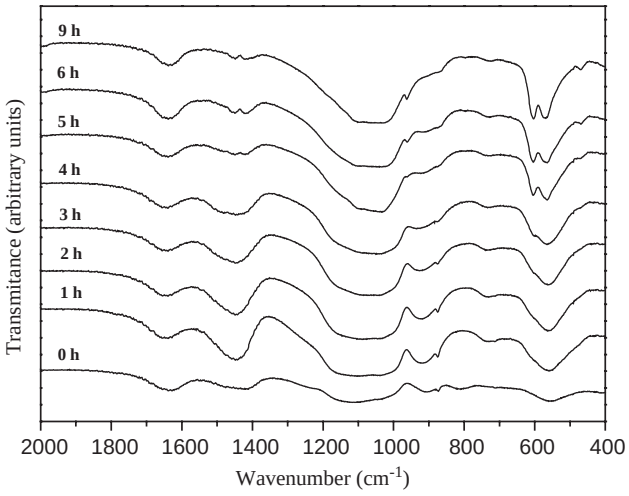

Fig. 4. The IR spectra of the untreated and mechanochemically treated mixture of $Ca(OH)_2$–P_2O_5–CaF_2.

Table 3
Assignment of IR absorption bands

Mode	Sample			
	FA ($t = 6$ h)	FA ($t = 9$ h)	FA ($t = 6$ h, 1100°C)	FA ($t = 9$ h, 1100°C)
ν_3(O–H)	3430	3430	3430	3430
	2926	2926	2926	2926
δ(O–H)	1626	1626	1626	1626
$\nu_3(CO_3^{2-})$	1455	1455	—	—
$\nu_3(CO_3^{2-})$	1420	1420	—	—
$\nu_3(PO_4^{3-})$	1092	1092	1093	1093
$\nu_3(PO_4^{3-})$	1046	1042	1043	1043
$\nu_1(PO_4^{3-})$	963	962	963	963
ν ($FHOOHF^-$)	726	726	—	726
ν_L(O–H)	—	—	630	—
$\nu_4(PO_4^{3-})$	603	603	603	603
$\nu_4(PO_4^{3-})$	571	571	571	571
$\nu_2(PO_4^{3-})$	473	473	473	473

agreement with the curent study, showing that almost pure fluorapatite was obtained.

Also, besides the band at 726 cm^{-1} an additional vibration at 630 cm^{-1} appears for the samples milled for 6 h and thermally treated up to 1100°C. As seen in the literature [23–29], this vibration originates from the OH^- liberation vibration mode and shows that hydroxyapatite is still present in the sample and thus showing the incompleteness of fluoroapatite formation. Also, the absence of the band at 630 cm^{-1} and the appearance of the band at 758 cm^{-1} in the samples treated mechanochemically for 9 h and then thermally (Fig. 5b and Table 3), indicates complete transformation of carbonated fluorhydroxyapatite (FHA) into fluoroapatite (FA).

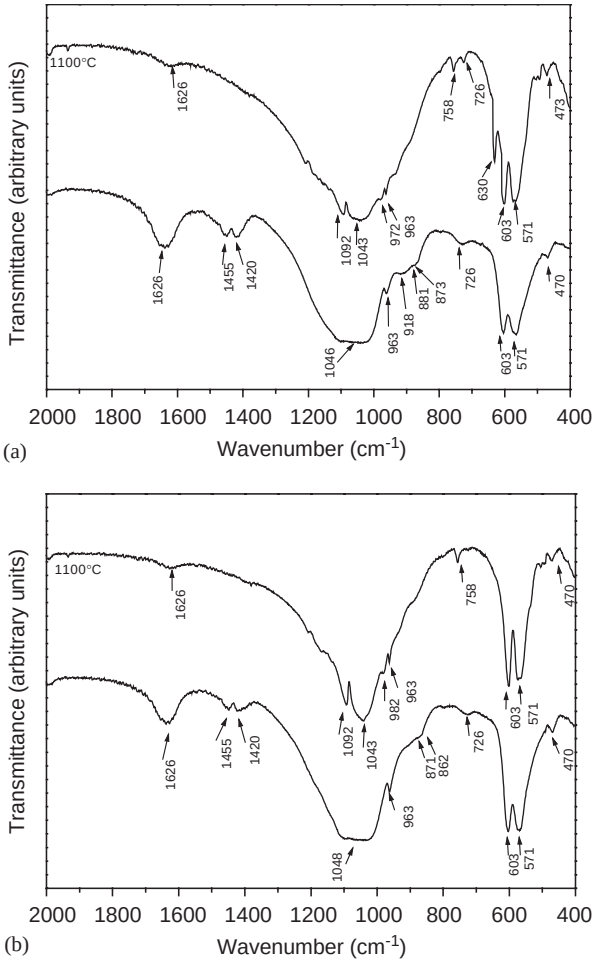

Fig. 5. The IR spectrum of the mechanochemically treated mixture of $Ca(OH)_2$–P_2O_5–CaF_2 for different milling time: (a) 6 h and (b) 9 h, before and after the thermal treatment process.

3.4. Scanning electron microscopy

Morphology of the starting powder components used for the mechanochemical treatment is illustrated in Fig. 6. As evident from microphotographs, the CaF_2 powder consists basically of large, prismatic/cubic agglomerates/particles, 10–20 μm in size. $Ca(OH)_2$ consists of two types of agglomerates/particles: polygonal ones similar in size to fluorite particles, and particles 1–3 μm in size bonded into clusters (Figs. 6a and b).

No significant changes in size distribution and morphology of the agglomerates/particles can be observed in microphotographs of the samples mechanochemically treated between 1 and 9 h (Figs. 7a–d). This is especially valid for the largest particles. Only accumulated fine particles and laminae of polygonal shape are visible on the surfaces of larger particles.

As evident from Figs. 7a–d, agglomerates of all samples are sized from 5 to 25 μm. Fine agglomerates consist of significantly finer agglomerates/particles

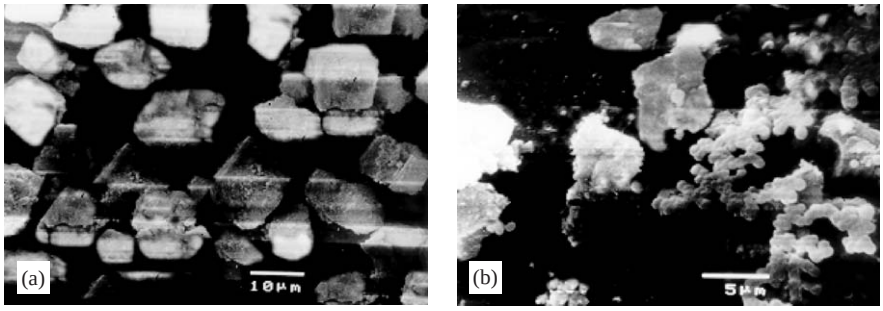

Fig. 6. The SEM micrographs of the initial components: (a) CaF_2, (b) $Ca(OH)_2$.

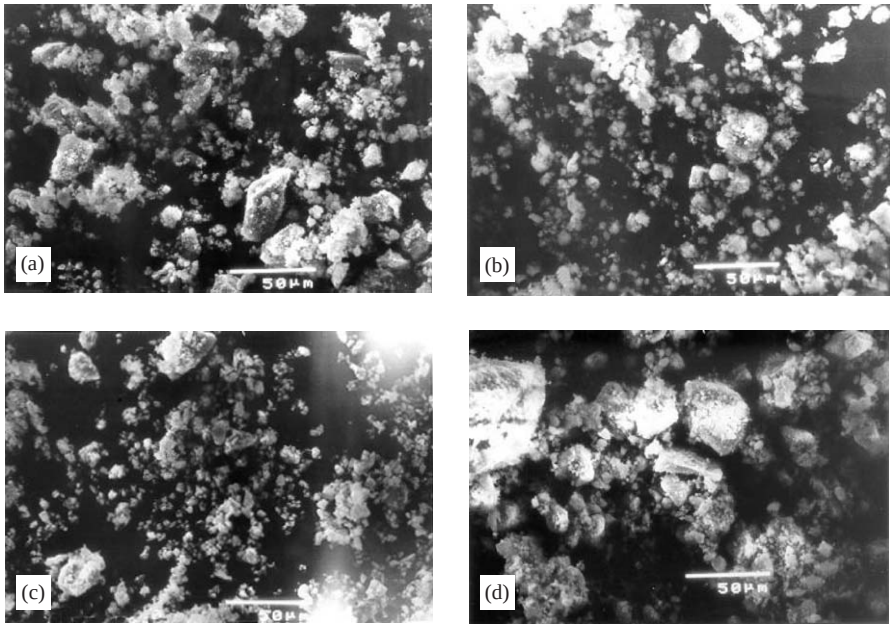

Fig. 7. SEM micrographs of the samples milled for: (a) 2 h, (b) 5 h, (c) 6 h and (d) 9 h; magnification is 500 × .

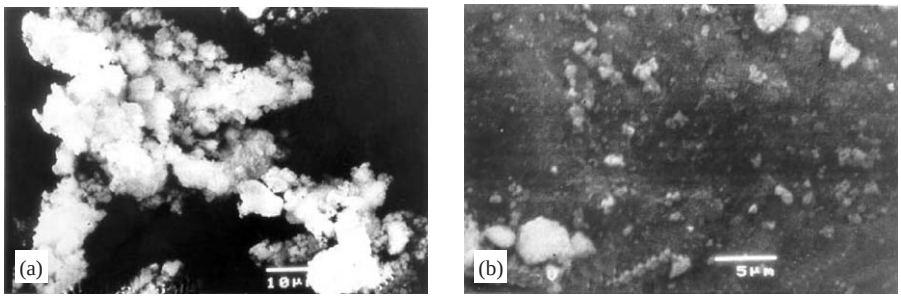

Fig. 8. SEM micrographs of characteristic details of the fine agglomerates and particle gatherings: (a) samples after 5 h milling and (b) samples after 9 h milling.

(Figs. 8a and b) that cannot be seen individually in microphotographs because of their exceptionally small sizes. Very fine accumulated particles, 1–5 μm in size, are also evident. In addition, the micrographs give us an idea about fine agglomerates of particles interconnected, in different ways, into structures of different forms, morphology and distribution.

No significant differences in the particle size distribution can be observed in microphotographs of the samples milled for the given period of time. Even the particles agglomerated into larger blocks at the beginning of the milling (Fig. 7a), bonded during further milling finer particles to themselves, forming round agglomerates (Fig. 7d), which, compared with the 2 h

milled sample, exhibit higher degree of cohesion. As also evident from microphotographs, outside surfaces and edges of grains are not crushed.

Homogeneity of composition is determined by EDS and F^- Ion selective electrode analysis by measuring concentration ratios of Ca, P and F from various parts of sample. This confirmed that a very homogeneous distribution of components is formed during mechanochemical treatment in all parts of the sample. It was found that there are no side effects, such as migration of F^- ions, even in systems which were thermally treated, because in the previous step (mechanochemical treatment) F^- ions were built into the FA lattice. Possibly only a redistribution of F^- ions between CaF_2 and FA takes place, while the total content of F^- remains constant through the end of the process.

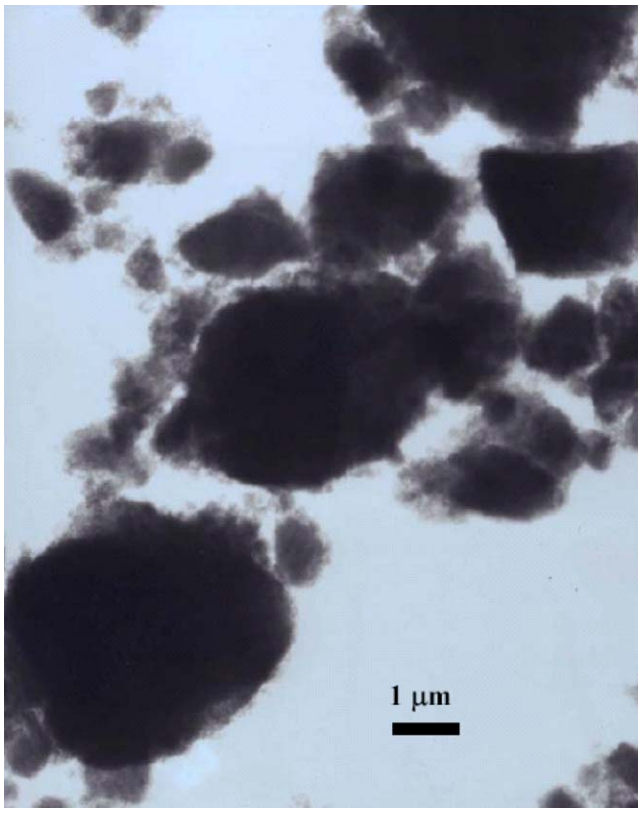

Fig. 9. TEM micrograph of the $Ca(OH)_2$–P_2O_5–CaF_2 mixture milled for 9 h shows agglomerates of small particles.

3.5. Transmission electron microscopy

Fig. 9 illustrates a detailed insight into the morphology of the powder obtained by milling for 9 h. The FA powder is highly agglomerated. Agglomerates, 5–40 μm in size, have frequently polyhedron shapes with curved corners and geometrically well defined surfaces.

At higher magnifications, it is evident that agglomerates consist of smaller particles, from approximately 25 to 100 nm in size (Fig. 10a). The electron diffraction pattern recorded for the region of small particles (Fig. 10b) corresponds to the fluoroapatite structure.

The electron diffraction pattern of the experimentally selected area was composed of reflections (spots) originating from individual particles. All of the reflections could be indexed according to the fluoroapatite structure. The reflections of the experimental pattern are connected to rings at the positions where the calculated powder electron diffraction pattern shows the highest intensity: (210), (211) and (213). Those positions are marked on the experimental diffraction pattern in Fig. 10b. The reflections are broadened and diffuse, due to the small particle size.

3.6. Differential thermal analysis

The DTA curves of the constituent phases of $Ca(OH)_2$–P_2O_5–CaF_2 powder mixture for 6 and 9 h of milling are shown in Fig. 11.

(a) (b)

Fig. 10. TEM micrograph (a) and corresponding electron diffraction pattern (b) of the small particles in the $Ca(OH)_2$–P_2O_5–CaF_2 mixture milled for 9 h. The electron diffraction pattern was indexed on the basis of fluoroapatite structure.

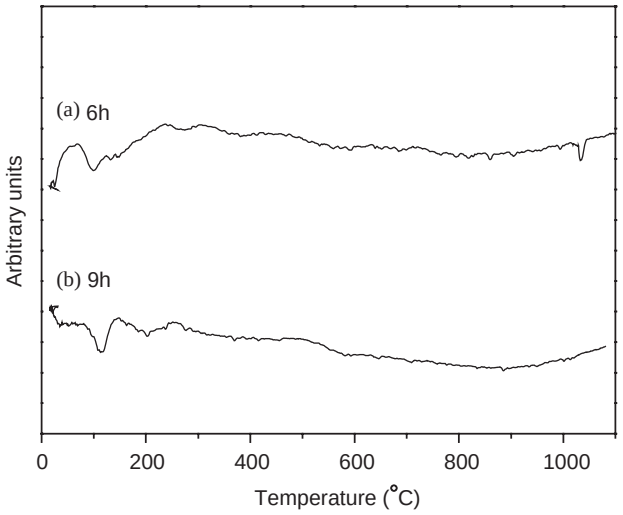

Fig. 11. DTA curves of the $Ca(OH)_2$–P_2O_5–CaF_2 mixture milled for different duration: (a) 6 h, (b) 9 h.

The DTA graph for the mixture milled 6 h shows a peak at 1050°C, which corresponds to the pyrolysis of carbonate from calcium hydroxyapatite. It is not seen in the sample milled for 9 h. However, in this sample, there are two new endothermic peaks at 120°C and 200°C, for the sample milled for 9 h, which correspond to the loss of physically adsorbed water.

4. Discussion

4.1. Reaction mechanism

According to considerations given in previous chapter concerning the data obtained by IR spectroscopy, DTA and XRD analysis, and SEM microscopy for the mechanochemically treated $Ca(OH)_2$, P_2O_5 and CaF_2 powders, the following reaction mechanism steps (transformations of the reactants involved) have been postulated.

After the beginning of milling (during the first hour of milling):

$$Ca(OH)_{2-2y}(CO_3)_y + (1-y)H_3PO_4 \rightarrow Ca(HPO_4)_{1-y}(CO_3)_y + (2-2y)H_2O, \quad (1a)$$

$$CaF_2 + H_3PO_4 \rightarrow CaHPO_4 + 2HF. \quad (1b)$$

From 1 up to 4–5 h of milling:

$$6Ca(HPO_4)_{1-y}(CO_3)_y + 3Ca(OH)_2 + 5yH_3PO_4 + xHF \rightarrow Ca_9(HPO_4)_{1-y}(CO_3)_y(PO_4)_5(OH)_{1-x}(F)_x + 5yH_2CO_3 + (5+x)H_2O. \quad (1)$$

During 4–6 h of milling:

$$Ca_9(HPO_4)_{1-y}(CO_3)_y(PO_4)_5(OH)_{1-x}(F)_x + CaF_{2-x} + (1-x)H_2O + (y-x)H \rightarrow Ca_{10}(PO_4)_{1-y}(CO_3)_y(PO_4)_5(OH)_{2-2x}(F)_{2x} + (2-2x)HF. \quad (2)$$

During 4–9 h of milling:

$$Ca_{10}(PO_4)_{1-y}(CO_3)_y(PO_4)_5(OH)_{2-2x}(F)_{2x} + (2-2x)HF \rightarrow Ca_{10}(PO_4)_{1-y}(CO_3)_y(PO_4)_5F_2 + 2(1-x)H_2O. \quad (3)$$

Suggested reactions mainly proceed with incomplete stoichiometry, wherein the value x defines the deviation from the complete stoichiometry, within the interval $(x_1; x_k); x_1 < x < x_k$, where x_k can have the maximum value of 1, and x_1 the minimum value of 0.

$$Ca_{10}(PO_4)_{1-y}(CO_3)_y(PO_4)_5(OH)_{2-2x_1}(F)_{2x_1} + (2-2x_1)HF \rightarrow Ca_{10}(PO_4)_{1-y}(CO_3)_y(PO_4)_5(OH)_{2-2x_k}F_{2x_k} + (2-2x_k)HF + 2(x_k-x_1)H_2O. \quad (4)$$

Consequently, the stoichiometry for the overall reaction of mechanochemical synthesis will be,

$$Ca(OH)_{2-2y}(CO_3)_y + (3-y/2)P_2O_5 + 8Ca(OH)_2 + CaF_2 + 3y/4O_2 \rightarrow Ca_{10}(PO_4)_{1-y}(CO_3)_y(PO_4)_5F_2 + (9-y)H_2O;\ x=1. \quad (5)$$

It can be concluded, based on XRD data, that partial amorphyzation of the system occurred already after 1 h of milling. Namely, the exceptionally high mechanical stress concentration over a very small contact area (contacts between the balls on their impacts, or on impacts of the balls against inner walls), provides conditions for the generation of a high strain gradient over a relatively small contact surface area. The deformation strain depends primarily on the radii of the balls used for mechanochemical treatment and the impact velocity. The deformation penetrates through the particle/particle assembly by means of dislocation mechanisms (sliding and climbing) of high velocity, i.e., via impact waves [35]. During mechanochemical process chemical and phase changes occur due to the transfer of deformations with high elastic flow. Due to high elastic flow, the prevailing mechanism is creeping, while the specified changes can be completely irreversible. Critical creeping strain in the milling materials depends on the time the system was exposed to deformation (for example number of ball impacts or number of stress cycles applied on the material). Therefore, the strain, which provokes the critical deformation and fractures that form new surfaces, will decrease gradually as the process proceeds, leading to a highly amorphous system. The process of mechanochemical activation of the systems, which generates

water as a reaction product, is additionally accelerated by an alleviated transport of the corresponding ions to the reaction zone. This minimizes the Gibbs free energy of the overall reaction of mechanochemical synthesis.

Due to very high hydrophilicity of P_2O_5, phosphoric acid ($P_2O_5 + 3H_2O \rightarrow 2H_3PO_4$) is formed immediately upon addition of P_2O_5 to the reaction mixture. The H_3PO_4 then reacts with $Ca(OH)_{2-2y}(CO_3)_y$ according to reaction (1).

The presence of carbonated calcium-hydrogen phosphate $Ca(HPO_4)_{1-y}(CO_3)_y$ is confirmed by bands at 875 and 918 cm^{-1} in the IR spectrum of the milled product (band for HPO_4^{2-} group). In addition, another simultaneous reaction occurs:

$$CaF_2 + H_3PO_4 \rightarrow CaHPO_4 + 2HF. \quad (6)$$

After 2 h milling the appearance of the band at 726 cm^{-1} indicates that the configuration FHO:OHF is predominant in (OH^-, F^-) apatite chains. In accordance to this, almost half of the OH^- ions are replaced with F^-. The propagation of the reaction is very slow which is shown by the presence of the band in the same place for 2 and 6 h.

After 2 h (and especially after 4 h) of milling, characteristic bands for HPO_4^{2-} become less and less intense, disappearing completely after 5 h. Also, the appearance of a new band at 963 cm^{-1} indicates formation of carbonated calcium-deficient hydroxyfluorapatite $Ca_9(HPO_4)_{1-y}(CO_3)_y(PO_4)_5(OH)_{1-x}(F)_x$, according to reaction (2). This reaction becomes dominant, replacing the reaction of $Ca(HPO_4)_{1-y}(CO_3)_y$ formation. The apatite subsequently reacts with the remaining $Ca(OH)_{2-2y}(CO_3)_y$, according to reaction (3), forming $Ca_{10}(PO_4)_{1-y}(CO_3)_y(PO_4)_5(OH)_{2-2x}(F)_{2x}$. This reaction is accompanied by HPO_4^{2-} deprotonation, as confirmed by disappearance of the band at 918 cm^{-1} and appearance of the band at 963 cm^{-1}.

Dissociation of CaF_2 takes place during the whole mechanochemical process, generating F^- ions, which react with stoichiometrically deficient calcium-hydroxyfluorapatite. Dissociation of calcium-fluoride results from the chemical reaction within the system defects (open surfaces, corrosion pits, dislocations, dislocation loops, vacancies, etc.). The corrosion tears the Ca^{2+} ions away, leaving bare F^- ions, which are carried by water molecules to the places that correspond to the given concentration gradient at the local surface. Therefore, it is realistic to assume that any of the involved reactions advance differently in larger and smaller initial particles of the reactants, reaching equilibrium in different times.

The band at 963 cm^{-1} appearing after 5 h of milling indicates continuous deprotonation of HPO_4^{2-}, although reaction (3) becomes dominant after 4 h of milling.

There are no bands at 1420 and 1455 cm^{-1} (ascribed to CO_3^{2-}) for the powder mixtures mechanochemically treated for 6 and 9 h and then thermally at 1100°C. But, a new band at 630 cm^{-1} appears, for the mixtures milled for 6 h, indicating incomplete exchange of the hydroxyl group for fluorine. The band at 726 cm^{-1}, present all the time for all milled powders, probably indicates no significant changes in F^- coordination during F^- transfer from CaF_2 into calcium-hydroxyfluorapatite. Also, consequently to considerations in the previous chapter, it appears that almost half of mixture is transformed into the fluoroapatite in samples milled 4 h and more.

The rate of HPO_4^{2-} deprotonation and of OH^- and F^- exchange controls the rate of fluoroapatite formation throughout the milling process. As the mechanical alloying progresses, calcium fluoride dissociation becomes its main limiting factor.

Reaction products on the surfaces of larger particles probably form soon after the process started, while the particles deep inside, remain unchanged. The morphology of particles is the same, even after longer milling times (4–6 h), confirming that the chemical process in each single particle or particle group advances independently.

In smaller particles, the mechanochemical process advances rapidly and after reaching equilibrium it continues infinitely slowly. Among regularly sized particles and especially in large ones the mechanochemical process proceeds with full intensity along the new-opened reaction fronts (new surfaces, crystallite edges and mosaic block rims).

As soon as reactions (2) and (3) become dominant in the studied system, crystallites start to grow becoming the main building blocks for the mechanochemically treated particles. This stage of the process commences after approx. 4 h (see the XRD pattern in Fig. 1) and then continues with increasing intensity, yielding (after 6 h) clearly distinguished crystallites, approx. 20 nm in size. Later on, these crystallites coalesce by means of surface interactions (clusters of vacancies) and dislocations [36,37].

The FHA/FA crystallization probably begins at the highest local deformation providing conditions for the formation of cell substructures. The nucleation and subsequent particle growth of the synthesized product correspond to the stoichiometry of the interactive ion species [36,37].

Assuming that the deformation process propagates at a velocity of approx. 190–950 m/s [35], the crystallite sizes, calculated by the Scherer formula, have values in the range from 5 to 31 nm. Similar values of approx. 10 nm were also confirmed by TEM analysis.

5. Conclusion

The experimental results obtained for the mechanochemical synthesis of carbonated calcium-fluoroapatite led to the following conclusions:

The synthesis proceeds in several steps. In the first step $Ca(HPO_4)_{1-y}(CO_3)_y$ is formed, as confirmed by IR bands at 875 and 918 cm^{-1} for HPO_4^{2-}. This reaction is dominant during the first 4 h of mechanochemical treatment. The synthesis progresses via partial dissociation of calcium fluoride, during which $Ca_9(HPO_4)_{1-y}(CO_3)_y(PO_4)_5(OH)_{1-x}(F)_x$ is generated, followed by disappearance of IR bands for HPO_4^{2-} and appearance of the band at 963 cm^{-1} for PO_4^{3-}, and the band at 726 cm^{-1} which is characteristic for equimolar hydroxyapatite/fluoroapatite mixture.

After 5 h of milling, the formation of $Ca_{10}(PO_4)_{1-y}(CO_3)_y(PO_4)_5(OH)_{2-2x}(F)_{2x}$ becomes dominant, followed by complete disappearance of the band characteristic of HPO_4^{2-}.

Prolonged milling time increases the content of F^- substituted in calcium hydroxyapatite. This causes the appearance of the band at 758 cm^{-1}. For sample mechanochemically treated for 9 h followed by unisothermal treatment up to 1100°C, only the band at 758 cm^{-1} appears thus confirming complete exchange of OH^- ions for F^-.

After 4 h of milling, stoichiometrically deficient carbonated hydroxyfluorapatite—$Ca_9(HPO_4)_{1-y}(CO_3)_y(PO_4)_5(OH)_{1-x}(F)_x$—was formed. By subsequent mechanochemical treatment up to 9 h, crystallites grew through a coalescence mechanism to the size of 31 nm.

The calculated values for the lattice parameters deviate insignificantly from one another as well as from the standard lattice parameter values.

The process of mechanochemical milling advances differently in larger and smaller particles due to different accessibility of the respective reactive surface areas.

Taking into account the estimated crystallite size of FHA and FA synthesized by mechanochemical process, it can be concluded that the mechanochemical synthesis depends mainly on the rate of particle deformation and the velocity of impact waves.

Acknowledgments

This work was supported by the Ministry of Science and Technology of the Republic of Serbia through project No. 1431—"Molecular Designing of Monolithic and Composite Materials".

We would like to thank M. Miljković and Dj. Janaćković for help and support.

References

[1] D.Mc. Connell, in: Apatite: Its Crystal Chemistry, Mineralogy, Springer, New York, 1973.
[2] L.L. Hench, J. Am. Ceram. Soc. 74 (7) (1991) 1487–1510.
[3] L.L. Hench, J. Am. Ceram. Soc. 81 (7) (1998) 1705–1728.
[4] R.Z. LeGeros, J.P. LeGeros, in: L.L. Hench, J. Wilson (Eds.), An introduction to Bioceramics, Adv. Ser. Ceram. Vol. 1, World Scientific Publishing Co. Pvt. Ltd., London, Hong Kong, Singapure, 1998, pp. 139–180.
[5] T. Kanazawa, T. Umegaki, K. Yamashita, H. Monma, T. Hiramatsu, J. Mater. Sci. 26 (1991) 417–422.
[6] I. Manjubala, M. Sivakumar, S. Najma Nikkath, J. Mater. Sci. 36 (2001) 5481–5486.
[7] J. Carsten, B. Marco, Biomaterials 17 (1996) 2065–2069.
[8] W.J.A. Dhert, P. Thomson, C.P.A.T. Klein, K. De Groot, P.M. Rozing, L.E. Ericson, J. Mater. Sci: Mater. Med. 5 (1994) 59–66.
[9] K. Cheng, W. Weng, G. Han, P. Du, G. Shen, J. Yang, J.M.F. Ferreira, Mater. Chem. Phys. 78 (2003) 767–771.
[10] M. Diarra, G. Pourroy, C. Boymond, D. Muster, Biomaterials 24 (2003) 1293–1300.
[11] N. Ignjatović, S. Tomić, M. Dakić, M. Miljković, M. Plavšić, D. Uskoković, Biomaterials 20 (1999) 809–816.
[12] M. Asada, Y. Miura, A. Osaka, K. Okkami, S. Nakamura, J. Mater. Sci. 23 (1988) 3202–3205.
[13] A. Slosarczyk, E. Stobierska, Z. Paszkiewicz, M. Gawlicki, J. Am. Chem. Soc. 79 (1996) 2539–2544.
[14] H. Monma, T. Kamiya, J. Mater. Sci. 22 (1987) 4247–4250.
[15] S. Lazić, S. Zec, N. Miljević, S. Milonjić, Thermochim. Acta 374 (2001) 13–22.
[16] S.R. Kim, J.H. Lee, Y.T. Kim, D.H. Riu, S.J. Jung, Y.J. Lee, S.C. Chung, Y.H. Kim, Biomaterials 24 (2003) 1389–1398.
[17] D.j. Janaćković, I. Petrović-Prelević, L.j. Kostić-Gvozdenović, R. Petrović, V. Jokanović, D. Uskoković, Bioceramics 13 (2001) 192–195.
[18] S.R. Kim, J.H. Lee, Y.T. Kim, D.H. Riu, S.J. Jung, Y.J. Lee, S.C. Chung, Y.H. Kim, Biomaterials 24 (2003) 1389–1398.
[19] R.N. Panda, M.F. Hsieh, R.J. Chung, T.S. Chin, J. Phys. Chem. Solids 64 (2003) 193–199.
[20] L.M. Rodriguez-Lorenzo, J.N. Hart, K.A. Gross, Biomaterials 24 (2003) 3777–3785.
[21] M. Wei, J.H. Evans, T. Bostrom, L. Grøndahl, J. Mater. Sci.: Mater. Med. 14 (2003) 311–320.
[22] M. Okazaki, Y. Miake, H. Tohda, T. Yanagisawa, J. Takahashi, Biomaterials 20 (1999) 1303–1307.
[23] M. Okazaki, Y. Miake, H. Tohda, T. Yanagisawa, T. Matsumoto, J. Takahashi, Biomaterials 20 (1999) 1421–1426.
[24] I. Nikčević, M. Mitrić, Z. Nedić, D. Uskoković, in: M.V. Nikolić (Ed.), Science of Sintering: Current Problems and New Trends, Serbian Academy of Sciences and Arts, Belgrade, 2003, pp. 209–218.
[25] K.C.B. Yeong, J. Wang, S.C. Ng, Biomaterials 22 (2001) 2705–2712.
[26] Sang-Hoon Rhee, Biomaterials 23 (2002) 147–1152.
[27] W.L. Suchanek, P. Shuk, K. Byrappa, R.E. Riman, K.S. TenHuisen, V.F. Janas, Biomaterials 23 (2002) 699–710.
[28] J. Liao, K. Hamada, M. Senna, J. Mater. Synth. Process. 8 (2000) 305–311.
[29] T. Isobe, S. Nakamura, R. Nemoto, M. Senna, H. Sfihi, J. Phys. Chem. B 106 (2002) 5169–5176.
[30] H. Rietveld, J. Appl. Crystallogr. 2 (1969) 65–71.
[31] R.W. Cheary, A.A. Coelho, J. Appl. Crystallogr. 25 (1992) 109–121.
[32] R.A. Nyquist, R.O. Kagel, Infrared Spectra of Inorganic Compounds, (3800–45 cm^{-1}), Academic Press, New York, London, 1971, p. 493.
[33] K. Nakamoto, Infrared and Raman Spectra of Inorganic and Coordination Compounds, Wiley, New York, Chichester, Brisbane, Toronto, 1978.
[34] F. Freund, R.M. Knobel, J. Chem. Soc. Dalton (1977) 1136–1140.
[35] M.V. Chaikina, in: E.G. Avvakumov (Ed.), Mehanohimija prirodnih i sinteticheskih apatitov, Novosibirsk, Izdatelstvo so ran, Filial "Geo", 2002.
[36] R.M. German, Sintering Theory and Practice, Wiley-Interscience Publication, New York, 1996.
[37] W.D. Kingery, H.K. Bowen, D.R. Uhlmann, Introduction to Ceramic, Wiley-Interscience Publikation, New York, 1976.